RSC Advances

ROYAL SOCIETY OF CHEMISTRY

www.rsc.org/advances

Journal Name

ARTICLE

Surface modification of $LiNi_{0.5}Mn_{1.5}O_4$ cathode with lithium boron oxide glass for lithium-ion batteries

Received 00th January 20xx,
Accepted 00th January 20xx

DOI: 10.1039/x0xx00000x

www.rsc.org/

Chenqiang Du[a], Man Yang[*, a], Jie Liu[a], Shuting Sun[a], Zhiyuan Tang[**, a], Deyang Qu[b], Xinhe Zhang[b]

Lithium boron oxide glass (LBO-glass) coated $LiNi_{0.5}Mn_{1.5}O_4$ cathode materials have been synthesized by a solution method to enhance the electrochemical performances. The structure and morphology of the as-prepared materials have been characterized by XRD, SEM, and TEM. The results indicate that the $LiNi_{0.5}Mn_{1.5}O_4$ is coated with a layer of amorphous LBO-glass. The electrochemical properties are characterized by galvanostatic charge-discharge cycling, cyclic voltammetry, electrochemical impedance spectroscopy and self-discharge test. Differential scanning calorimetry is carried out to confirm the improved safety by LBO-glass coating. The LBO coating can effectively enhance electrochemical kinetics of $LiNi_{0.5}Mn_{1.5}O_4$ phase and improve the cycling performance. Among the as-prepared samples, the 1 wt% LBO-glass coated $LiNi_{0.5}Mn_{1.5}O_4$ presents the optimal electrochemical behaviors with a capacity retention of 91.4% after 100 cycles at 1 C and a discharge capacity of 105.8 mAh g^{-1} at 10 C. Besides, the electrochemical impedance spectroscopy analysis shows the 1 wt% LBO-glass coating reduces the electrochemical impedance and improves the ability to conduct Li^+ of the cells to a great extent.

1. Introduction

Lithium-ion batteries have been successful for portable electronic devices such as cell phones and laptop computers due to their higher energy density compared to other rechargeable systems. Aggressive research has recently been focused on the development and optimization of advanced cathode materials for electric vehicles (EV) and hybrid electric vehicles (HEV). However, the existing battery technology established for portable electronics has faced great challenges to meet the criteria of the automotive applications, especially in terms of energy density. One effective strategy to increase energy density is to increase the operating voltage of the battery [1]. A series of high-voltage cathode materials ($LiM_xMn_{2-x}O_4$, M=Ni, Co, Cr, Cu, Fe) have been investigated in the pursuit of substituting transition metals (M) for the Mn site in $LiMn_2O_4$ [2], among which $LiNi_{0.5}Mn_{1.5}O_4$ has drawn much attention because of its high specific capacity (147 mAh g^{-1}) and high operating voltage (4.7 V vs. Li^+/Li).

However, the poor electrochemical performances of $LiNi_{0.5}Mn_{1.5}O_4$ such as low discharge capacity and depressed cyclability hinder its application to a large extent [3]. One reason is the decomposition of electrolyte at high operating voltage [4, 5], resulting in the formation of SEI film, which blocks the insertion/extraction of Li^+ and hinders the charge transfer, hence the kinetics of the electrochemical processes. Besides, side reactions between the cathode material and the electrolyte restrict its electrochemical performance [6]. Also, the minor Mn^{3+} ions in $LiNi_{0.5}Mn_{1.5}O_4$, which result from high-temperature and long-time calcinations, further lead to Mn dissolution, structure distortion, and capacity fading upon cycling [7]. To overcome these disadvantages, many efforts have been made, such as ion doping [8–20] and surface coating [21–29]. Cation and/or anion doping such as Zn^{2+} [8], Mg^{2+} [9, 10], Al^{3+} [11, 12], Fe^{3+} [13], Cr^{3+} [11, 14, 15], Sm^{3+} [16], Ru^{4+} [17, 18], Ti^{4+} [18], Nb^{5+} [19], W^{6+} [20] and F^- [11] have been employed to improve the electrochemical behaviours of $LiNi_{0.5}Mn_{1.5}O_4$. However, doping is not able to prevent the decomposition of the electrolyte and side reactions between cathode and electrolyte. In recent years, various oxides and phosphates have drawn researchers' attention because of facile synthesis methods and positive effects on the electrochemical properties of $LiNi_{0.5}Mn_{1.5}O_4$, such as ZnO [21, 22], ZrO_2 [23], ZrP_2O_7 [23], Al_2O_3 [6, 22], $ZnAl_2O_4$ [24], Bi_2O_3 [6, 22], SiO_2 [25], CuO [26], $YBaCu_3O_7$ [27], BiOF [28], $AlPO_4$ [22], and $FePO_4$ [29]. These previous literatures have reported that the surface-modifications using inorganic materials are effective to enhance the electrochemical performances and the thermal stability of the high-voltage $LiNi_{0.5}Mn_{1.5}O_4$ cathode system.

Nevertheless, these coating materials can form barriers to the movement of lithium ions due to low ion conductivity. According to Amatucci and co-workers' report [30], lithium boron oxide glass (LBO-glass) is particularly suitable for surface modification for the following reasons. First of all, molten LBO compositions exhibit good wetting properties with respect to ceramics. Not only the good wetting properties but also the

[a] Department of Applied Chemistry, School of Chemical Engineering and Technology, Tianjin University, Tianjin 300072, China; E-mail: 369469876@qq.com; Fax: (+86)769–83195372; Tel.: (+86)769–83017180
[b] McNair Technology Company Limited, Dongguan City, Guangdong 523700, P.R. China.

relatively low viscosity of LBO-glass in the molten state allow easy processing and result in even coverage with the use of a minimal amount of material. Secondly, LBO compositions have already been investigated as solid lithium ion conductors which show good ability to conduct Li^+ [31, 32]. Furthermore, electrochemical studies have shown that LBO coating is helpful for the 4 V positive electrode materials used in lithium-ion batteries such as $LiNi_{0.8}Co_{0.2}O_2$ [33], $LiNi_{1/3}Co_{1/3}Mn_{1/3}O_2$ [34], $LiMn_2O_4$ [35, 36], $Li_{1+x}Mn_2O_4$ [37].

In this paper, a surface modification method is conducted through coating LBO-glass on $LiNi_{0.5}Mn_{1.5}O_4$ in order to enhance its electrochemical performances. The results of various structure and electrochemical analyses show that the LBO-glass plays a protecting role on the surface of $LiNi_{0.5}Mn_{1.5}O_4$ cathode, thus improving the electrochemical behaviours of the cathode materials.

2. Experimental

2.1. Preparation of cathode materials

For the synthesis of $LiNi_{0.5}Mn_{1.5}O_4$ powders, a co-precipitation method was employed. Stoichiometric amounts of $Mn(CH_3COO)_2{\cdot}4H_2O$ (A.R., Guangdong Guanghua Sci-Tech Co, Ltd.) and $Ni(CH_3COO)_2{\cdot}4H_2O$ (A.R., Guangdong Guanghua Sci-Tech Co, Ltd.) were dissolved in deionized water, then oxalic acid solution containing 10% excessive $H_2C_2O_4{\cdot}2H_2O$ (A.R., Guangdong Guanghua Sci-Tech Co, Ltd.) was dropped slowly into the metal acetate solution under stirring. After being stirred for 6h, the precipitation was washed, centrifuged and then dried at 80°C. The dried binary metal oxalate were mixed with stoichiometric Li_2CO_3 (A.R., Guangdong Guanghua Sci-Tech Co, Ltd.) (5% excessive to compensate for the lithium evaporation during high temperature calcination), preheated at 450°C for 5 h, and then calcined at 800°C for 12 h with a heating rate of 3°C min^{-1}. The powder was grinded and denoted as LNMO.

The LBO-glass coated $LiNi_{0.5}Mn_{1.5}O_4$ was prepared using a solution method. $LiOH{\cdot}H_2O$ (A.R., Guangdong Guanghua Sci-Tech Co, Ltd.) and H_3BO_3 (A.R., Guangdong Guanghua Sci-Tech Co, Ltd.) were mixed in ethanol (A.R., Guangdong Guanghua Sci-Tech Co, Ltd.) with a molar ratio of 1:2. Then bare $LiNi_{0.5}Mn_{1.5}O_4$ was added into the solution, and the mixture was stirred and heated at 80°C until the solvent was completely evaporated. The powders were grinded, pressed into pellets and heated at 500°C for 10 h. The melting points of H_3BO_3 and $LiOH{\cdot}H_2O$ were 186°C and 445°C, respectively. Therefore, during heating the liquid H_3BO_3 and $LiOH{\cdot}H_2O$ could wet the surface of $LiNi_{0.5}Mn_{1.5}O_4$ and reacted with each other, producing the LBO-glass. After the mixture cooled to room temperature, the solid Li_2O-$2B_2O_3$ glass modified $LiNi_{0.5}Mn_{1.5}O_4$ powders were obtained. The weight ratios of the Li_2O-$2B_2O_3$ glass to the $LiNi_{0.5}Mn_{1.5}O_4$ powders in the modified samples were 0.5%, 1%, 2% and 3%, which were denoted as 0.005LBO-LNMO, 0.01LBO-LNMO, 0.02 LBO-LNMO and 0.03LBO-LNMO, respectively.

2.2. Physical characterization

The crystal structure of samples was identified by X-ray diffraction (XRD, Rigaku RINT2000) using Cu Kα radiation operated at 30 kV and 20 mA with a scanning speed of 4° min^{-1}, from 10° to 80°. The particle morphologies were observed using scanning electron microscope (SEM, Hitachi, S4800). The high resolution transmission electron microscope (HRTEM, JEM-2100F) was employed to observe the LBO-glass layer on the $LiNi_{0.5}Mn_{1.5}O_4$ material.

The thermal stability of the LNMO and 0.01LBO-LNMO was studied using differential scanning calorimetry (DSC-Perkin-Elmer Pyris 1 differential scanning calorimeter). After 2 charge/discharge cycles at 0.1 C rate, the cells were fully-charged and subsequently subjected to 1 h of trickle charge at constant voltage of 5.0 V to ensure the cathode material is completely delithiated. Then, the cells were introduced into a dry glove box and opened carefully and the cathode materials were recovered. The electrodes were slightly dried and then scratched to obtain the cathode material. 5–6 mg materials from each kind of electrodes were packed into small stainless steel DSC capsules and then hermetically sealed. The samples were scanned in the DSC equipment under nitrogen purging from room temperature to 400°C at a heating rate of 10°C min^{-1}.

2.3. Electrochemical measurements

Electrochemical evaluations of materials were performed with CR2032 coin cells. The positive electrode was prepared by mixing the cathode materials, Super-P, and polyvinylidene fluoride (PVDF) binder with weight proportion of 8:1:1 in N-methyl-2-pyrrolidone (NMP) to form slurry. Then the slurry was coated onto an aluminium foil, which severed as a current collector, followed by drying at 120°C for 12 h in a vacuum oven. Finally, the cathode material coated foils were pressed under 10 MPa for 1 min, with a final active material loading about 2.8–3.0 mg cm^{-2}. The cells were fabricated in a vacuum glove box filled with argon, with lithium plate as the negative electrode, polypropylene (Celgard®2300, Celgard Inc. USA) as separator, and 1M LiPF6 dissolved in ethylene carbonate (EC)/diethyl carbonate (DEC) (1:1, by volume ratio) as electrolyte.

The charge/discharge tests were performed in the voltage range of 3.5–5.0 V (vs. Li^+/Li) on an automatic batteries tester (Land CT 2001A, Wuhan, China). The cycling stability was measured at 1 C (1 C=147 mAh g^{-1}) for 100 cycles. And to test the rate performance of the samples, the cells were charged at 0.5 C and discharged at different rates. Cyclic voltammetry (CV) tests were conducted on an electrochemical workstation (CHI1040B, ChenHua, China) with a voltage range of 3.5–5.0 V (vs. Li^+/Li) at a scanning rate of 0.1 mV s^{-1}. The electrochemical impedance spectroscopy (EIS) analysis of LNMO and 0.01LBO-LNMO was carried out after the cells were charged and discharged at 1 C for 1 cycle and 30 cycles respectively, on an electrochemical workstation (Gamry PC14-750) in the frequency range of 100 kHz to 10 mHz. Self-discharge of LNMO and 0.01LBO-LNMO was investigated on an electrochemical workstation (CHI1040B, ChenHua, China). The cells made by

LNMO and 0.01LBO-LNMO were charged and discharged at 0.1 C (1 C= 146.7 mA g^{-1}) in the voltage range of 3.5-5.0 V for 5 cycles, then charged to 5 V and left at open-circuit voltage for 10 days. All electrochemical measurements have been performed at room temperature.

3. Results and discussion

3.1. Physical characterization

The XRD patterns of pristine and LBO-glass coated $LiNi_{0.5}Mn_{1.5}O_4$ are shown in Fig. 1. All of the samples show sharp peaks of similar location and intensity, and these peaks can be well indexed to the spinel structured LNMO (JCPDS card No.80-2162, Fd-3m phase). It can be seen that there are weak peaks at 37.5°, 43.6° and 63.3° in the patterns of samples attributed to the secondary phases $Li_xNi_{1-x}O$, which is a common phenomenon in the preparation of $LiNi_{0.5}Mn_{1.5}O_4$. As previous literature reports[38-40], when the annealing temperature is above 650°C, $LiNi_{0.5}Mn_{1.5}O_4$ phase suffers a decomposition reaction as shown in equation (1), while the $Li_xNi_{1-x}O$ phase has no negative effects on the electrochemical performance of $LiNi_{0.5}Mn_{1.5}O_4$[41]. As a result, oxygen deficiency occurs and to maintain charge balance, some Mn^{3+} ions appear instead of Mn^{4+} ions, which is helpful to improve the electronic conductivity of $LiNi_{0.5}Mn_{1.5}O_4$[38]. The peaks of LBO cannot be detected, which is probably due to the low proportion of the LBO-glass or its amorphous nature [33].

$LiNi_{0.5}Mn_{1.5}O_4 \rightarrow \alpha\ Li_xNi_{1-x}O + \beta\ LiNi_{0.5-y}Mn_{1.5+y}O_4 + \gamma\ O2$ (1)

Fig. 2 shows the SEM images of the pristine and LBO-glass coated $LiNi_{0.5}Mn_{1.5}O_4$. It can be seen that the pristine $LiNi_{0.5}Mn_{1.5}O_4$ possesses a distribution of secondary particles sizing between 2–8 μm, while the LBO-glass coated materials possess a part of smaller secondary particles and slighter particle agglomerations. Thus, the LBO-glass coating prevents the aggregation of nanoparticles, which benefits the improvement of the electrochemical properties.

The HRTEM image of the 0.01LBO-LNMO is displayed in Fig. 3. It is observed that a thin film with a thickness in the range of 5–10 nm is coated on the surface of $LiNi_{0.5}Mn_{1.5}O_4$ cathode material. In addition, the fast Fourier transform (FFT) images are shown in the insets of Fig. 3, which confirm the crystalline characteristics of the $LiNi_{0.5}Mn_{1.5}O_4$ and the amorphous structure of the coated LBO-glass layer, in accordance with the XRD analysis. The lattice fringe with a d-spacing value of 0.4765 nm corresponds to the (111) plane of $LiNi_{0.5}Mn_{1.5}O_4$. From the TEM image and the XRD patterns, it is concluded that the LBO-glass layer is amorphous rather than crystalline [33, 36].

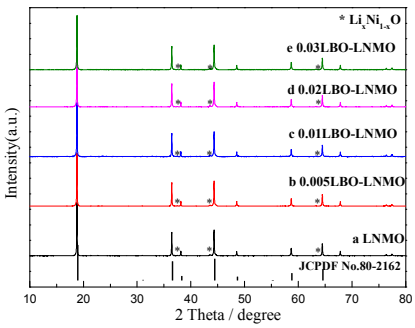

Fig. 1. XRD patterns of the pristine and LBO-glass coated $LiNi_{0.5}Mn_{1.5}O_4$

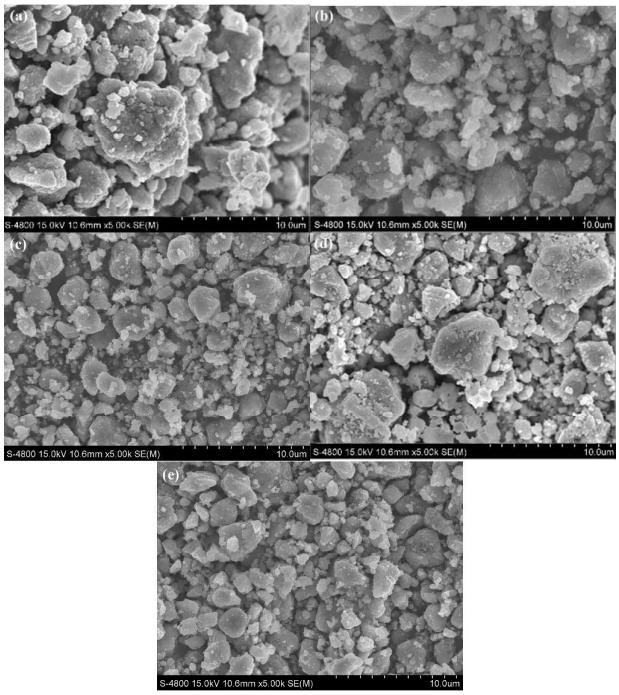

Fig. 2. SEM images of (a) LNMO, (b) 0.005LBO-LNMO, (c) 0.01LBO-LNMO, (d) 0.02LBO-LNMO, (e) 0.03LBO-LNMO

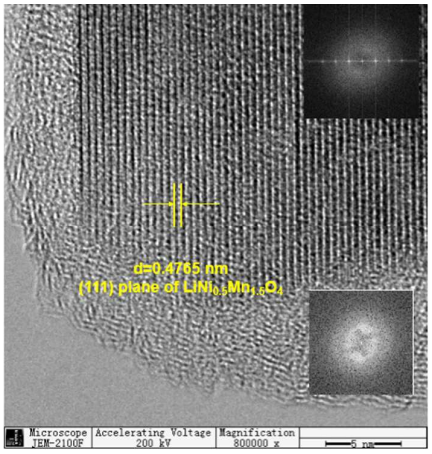

Fig. 3. HRTEM image of the 0.01LBO-LNMO

3.2. Electrochemical characterization

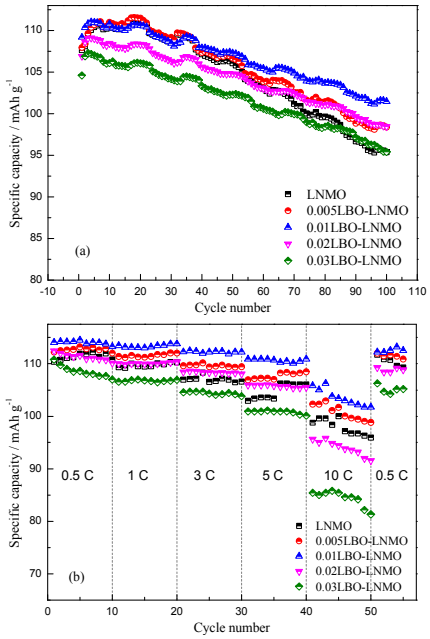

Fig. 4. Cycling performances for 100 cycles at 1 C (a) and rate performances (b) of the pristine and LBO-glass coated $LiNi_{0.5}Mn_{1.5}O_4$

Fig. 4 presents the cycling performances at 1 C rate (1 C=147 mAh g^{-1}) and rate performances of the pristine and LBO-glass coated $LiNi_{0.5}Mn_{1.5}O_4$. As seen in Fig. 4a, the discharge capacities of the samples show an increasing trend along with the cycle number at the initial several cycles. This should be attributed to the activation of the cells, which is a common phenomenon in the study of lithium-ion batteries and can be seen in previously reported literatures [42, 43]. The mass transfer is slower than the charge transfer under high current density. Therefore, during the initial cycles, some active materials are not involved in the charge/discharge process, leading to the low discharge capacities. After a few cycles of activation, the capacities gradually increase due to more and more active materials participating in the charge/discharge process. After several cycles, the LNMO, 0.005 LBO-LNMO, 0.01LBO-LNMO, 0.02LBO-LNMO and 0.03LBO-LNMO show the highest discharge capacities of 111.1, 111.5, 111.0, 109.1 and 107.3 mAh g^{-1}, respectively. While after 100 cycles, the corresponding capacities decrease to 94.3, 98.3, 101.5, 98.4 and 95.4 mAh g^{-1}, accompanied with a capacity retention of 85.9%, 88.1%, 91.4%, 90.2% and 89.0% compared with the highest discharge capacity, respectively. For the initial several cycles, the LBO-glass coated materials show lower discharge capacities compared with bare LNMO, which is caused by the electrochemical inactivity of the LBO-glass. However, the LBO-glass coated materials show higher discharge capacities and capacityretentions after 100 cycles at 1 C, indicating that LBO-glass layer plays a protecting role on the surface of the $LiNi_{0.5}Mn_{1.5}O_4$ materials, prevents the side reactions between cathode materials and electrolyte, stabilizes the structure of the cathode materials and thus improves the cycling stability.

To characterize the rate capability of the samples, electrodes made from the as-prepared materials are charged to 5.0 V at 0.5 C and discharged to 3.5 V at different rates from 0.5 C to 10 C and then back to 0.5 C. It can be clearly seen that the 0.01LBO-LNMO possesses the best rate capability and cyclability. A discharge capacity of 105.8 mAh g^{-1} can be retained at a discharge rate of 10 C for 0.01LBO-LNMO, while the LNMO, 0.005LBO-LNMO, 0.02LBO-LNMO and 0.03LBO-LNMO deliver lower capacities of 98.7, 102.3, 95.6 and 85.4 mAh g^{-1}, respectively. When the current density is reduced to 0.5 C, the discharge capacities could recover to their initial value, which indicates that rapid lithiation/delithiation and a large current density did not result in structural damage of the crystals. Moreover, both the stable structure and the LBO-glass with fast lithium ion conduction can reduce the polarization especially at high current density, which leads to an improvement of the rate capability. The worse discharge capacity of the 0.02LBO-LNMO and 0.03LBO-LNMO may be induced by the electrochemical inactivity of the excessive LBO-glass. It can be concluded that 1 wt% is a proper coating amount for the LNMO cathode material.

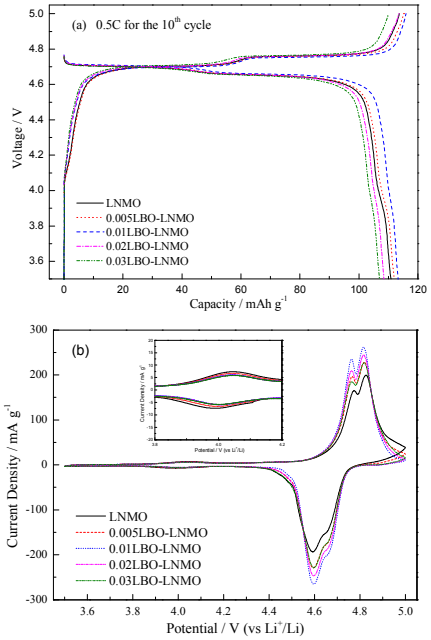

Fig. 5. Typical charge-discharge profiles (a) and cyclic voltammogram (CV) curves at a scanning rate of 0.1 mV s^{-1} (b) for the pristine and LBO-glass coated $LiNi_{0.5}Mn_{1.5}O_4$

Typical charge-discharge profiles at 0.5 C for the 10th cycle and cyclic voltammogram (CV) curves for the pristine and LBO-coated $LiNi_{0.5}Mn_{1.5}O_4$ at a scanning rate of 0.1 mV s^{-1} are shown in Fig. 5. As observed in Fig. 5a, two dominant plateaus around 4.7 V belonging to the charge curves are attributed to the redox reactions of Ni^{3+}/Ni^{2+} and Ni^{4+}/Ni^{3+} [29]. While for the discharge curves, only one distinct plateau is found around 4.7

V. As shown in Fig. 5b, two pairs of redox peaks (around 4.76/4.66 V and 4.81/4.67 V) are ascribed to the redox reactions of Ni^{3+}/Ni^{2+} and Ni^{4+}/Ni^{3+}, which is in accordance with the above results. Besides, a weak peak at around 4.0 V indicates the Mn^{4+}/Mn^{3+} redox reaction, which is in agreement with the magnified region in the CV curves. What's more, the 0.01LBO-LNMO presents a larger current density than other samples, suggesting a lower polarization of the material. On the basis of previous reports [31, 32], the LBO-glass is not a good electronic conductor, but a very good Li^+ ionic conductor. The thin coating layer may promote the Li^+ transfer process through the interfaces between the LBO-glass and the LNMO materials. As a result, the electrochemical polarization is decreased.

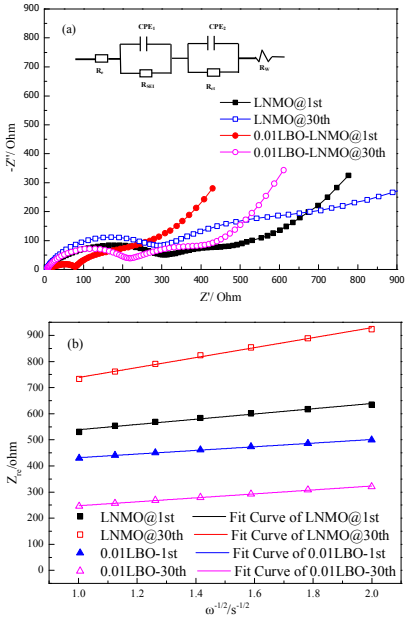

Fig. 6. Nyquist plots (a) and graph of Z_{re} plotted against $\omega^{-1/2}$ (b) of the LNMO and 0.01LBO-LNMO after cycled at 1C for 1 cycle and 30 cycles

Tab.1. Impedance parameters of the LNMO and 0.01LBO-LNMO

Samples	R_e / Ω	R_{SEI} / Ω	R_{ct} / Ω	σ/Ω·cm^2·s$^{-1/2}$	D/cm^2·s^{-1}
LNMO@1st	4.61	269.2	223.4	100.4	9.63×10^{-13}
LNMO@30th	4.01	295.3	333.1	190.7	5.07×10^{-13}
0.01LBO-LNMO@1st	5.48	60.4	81.1	65.6	1.47×10^{-12}
0.01LBO-LNMO@30th	4.43	183.5	170.3	75.6	1.28×10^{-12}

To further characterize the improved electrochemical behaviour of the 0.01LBO-LNMO, the EIS test results of the LNMO and 0.01LBO-LNMO are shown in Fig. 6. The resistances are evaluated using the equivalent circuit model shown in the inset of the Fig. 6a [23, 44, 45], and the fitted values are listed in Tab. 1. According to the literatures [23, 45], Re represents the solution resistance; R_{SEI} and CPE_1 signify the diffusion resistance of Li^+ through the solid-electrolyte interface (SEI) layer and the corresponding constant phase element (CPE); R_{ct} and CPE_2 correspond to the charge transfer resistance and the corresponding CPE, while R_W (not calculated here) is related to the solid-state diffusion of Li^+ in the active materials corresponding to the slope of the line at low frequency. From the fitted data, it can be concluded that the resistances of the electrolyte (R_e) are similar for both the LNMO and the 0.01LBO-LNMO. However, after 1 cycle at 1C, both the R_{SEI} and R_{ct} of the 0.01LBO-LNMO are much lower than those of the LNMO. Further, after the cells are charged and discharged for 30 cycles, R_{SEI} and R_{ct} show an increasement, which of the 0.01LBO-LNMO are still much smaller than that of that LNMO, indicating that the LBO-glass coating layer plays an important role in reducing the resistances. What's more, the EIS can also be used to calculate the lithium-ion diffusion coefficient (D) through employing the following equations [19, 26]:

$$Z_{re} = R_e + R_{ct} + \sigma\omega^{-1/2} \quad (2)$$

$$D = \frac{R^2T^2}{2A^2n^4F^4C_{Li}^2\sigma^2} \quad (3)$$

Where R is the gas constant, T is the absolute temperature (298.15 K), A is the surface area of the cathode (here the geometric area of electrode and it is 0.785 cm^2), n is the number of electrons transferred in the half-reaction for the redox couple of Ni^{4+}/Ni^{2+}, F is the Faraday constant, C_{Li} is the concentration of Li^+ in solid, and σ is the Warburg factor, which is relative to Z_{re}. The Z_{re}-$\omega^{-1/2}$ plots are presented in Fig. 6b. According to Eqs. (2) and (3), the lithium diffusion coefficients of the LNMO and 0.01LBO-LNMO are calculated to be approximate 9.63×10^{-13} and 1.47×10^{-12} cm^2 s^{-1} after 1 cycle at 1 C, 5.07×10^{-13} and 1.28×10^{-12} cm^2 s^{-1} after 30 cycles at 1 C, respectively. It is noticed that the diffusion coefficient of the cathode material is enhanced greatly by LBO-glass coating, which can be attributed to its ability to conduct lithium ions.

Self-discharge profiles of LNMO and 0.01LBO-LNMO cells are illustrated in Fig. 7. After storage for 10 days, the voltage of the charged LNMO cell decreases from 4.96 V to 4.70 V, while that of the 0.01LBO-LNMO decreases from 4.96 V to 4.74 V. It is apparent that the charged 0.01LBO-LNMO suffers less self-discharge than LNMO. Thus, LBO coating is an effective method to suppress this self-discharge, which may be attributed to the fact that LBO layer is able to protect the active material form reacting with the electrolyte and prevent the self-discharge.

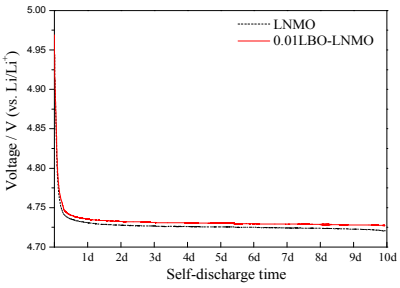

Fig. 7 Self-discharge profiles of LNMO and 0.01LBO-LNMO cells after 5 cycle at 0.1 C in the potential range of 3.5-5.0 V

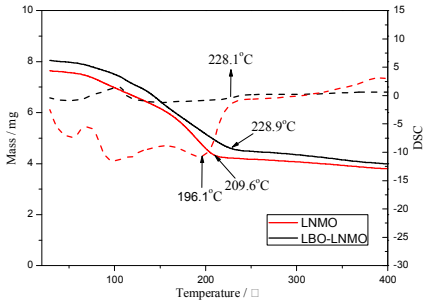

Fig. 8 DSC spectra of over charged LNMO and 0.01LBO-LNMO cathodes with traces of 1.0 mol L^{-1} LiPF6 in EC-EMC(3:7) electrolyte with a heating rate of 10°C min^{-1}

DSC spectra of over charged LNMO and 0.01LBO-LNMO are illustrated in Fig. 8. As shown in the Fig. 8, peaks around 100°C may be attributed to the decomposition of the trace of electrolyte. When the temperature reaches around 200°C, the cathodes undergo an exothermic reaction with large enthalpy and the reaction of LNMO gets completed at a much lower temperature than that of 0.01LBO-LNMO. Pristine $LiNi_{0.5}Mn_{1.5}O_4$ cathode is found to be thermally unsafe, while the coated one gain more thermal stability, which may be attributed to the fact that LBO glass improves the safety of the cathode material.

Conclusions

In summary, the $LiNi_{0.5}Mn_{1.5}O_4$ cathode materials were synthesized by a co-precipitation method and the LBO-glass coated $LiNi_{0.5}Mn_{1.5}O_4$ were synthesized by a solution method followed by heat treatment. The XRD patterns and TEM image indicate that the LBO-glass layer is amorphous. Cycling tests show the 0.01LBO-LNMO possesses the optimal electrochemical stability, which exhibits a capacity retention of 91.4% after 100 cycles at 1 C, higher than that of the LNMO, 0.005LBO-LNMO, 0.02LBO-LNMO and 0.03LBO-LNMO, corresponding 85.9% 88.1%, 90.2% and 89.0%, respectively. Furthermore, rate behaviour tests indicate that the 0.01LBO-LNMO holds the best rate performance and it keeps a discharge capacity of 105.8 mAh g^{-1} even at 10 C. The EIS and self-discharge results manifest that the LBO-glass layer not only acts as a Li^+ conductor, but also protects the electrode from corrosion by the electrolyte and prevents the reactions between electrolyte and cathode materials, reducing the impedance and the self-discharge of the cells. DSC data indicates that LBO coating improves the thermal safety of $LiNi_{0.5}Mn_{1.5}O_4$. Thus, LBO-glass surface modification is a promising way to improve the electrochemical properties of $LiNi_{0.5}Mn_{1.5}O_4$. As a promising extension, this LBO-glass coating method can be employed to improve other lithium-ion batteries materials.

Acknowledgements

This work is supported by the project of Innovative group for high-performance lithium-ion power batteries R&D and industrialization of Guangdong Province (Grant No. 2013N079).

Notes and references

1 Chong J, Xun S and Zhang J, *Chem Eur J*, 2014, 7479
2 Molenda J, Marzec J and Świerczek K, *Solid State Ionics*, 2004, **171**, 215
3 Yang T, Zhang N and Lang Y, *Electrochim Acta*, 2011, **56**, 4058
4 Yang L, Ravdel B and Lucht BL, *Electrochem Solid-State Lett*, 2010, **13**, A95
5 Xu K, *Chem Rev*, 2004, **104**, 4303
6 Liu J and Manthiram A, *J Electrochem Soc*, 2009, **156**, A833
7 Arrebola J, Caballero A and Hernan L, *J Electrochem Soc*, 2007, **154**, A178
8 Yang Z, Jiang Y and Kim JH, *Electrochim Acta*, 2014, **117**, 76
9 Liu MH, Huang HT and Lin CM, *Electrochim Acta*, 2014, **120**, 133
10 Liu G, Zhang L and Sun L, *Mater Res Bull*, 2013, **48**, 4960
11 Sha O, Tang Z and Wang S, *Electrochim Acta*, 2012, **77**, 250
12 Zhong GB, Wang YY and Zhang ZC, *Electrochim Acta*, 2011, **56**, 6554
13 Liu J and Manthiram A, *J Phys Chem C*, 2009, **113**, 15073
14 Xu H, Liu XJ and Peng QW, *Materials Express*, 2014, **4**, 72
15 Liu D, Lu Y and Goodenough JB, *J Electrochem Soc*, 2010, **157**, A1269
16 Mo M, Hui KS, Hong X and Guo J, *Appl Surf Sci*, 2014, **290**, 412
17 Wang H, Tan TA and Yang P, *J Phys Chem C*, 2011, **115**, 6102
18 Le MIP, Strobel P and Alloin F, *Electrochem Acta*, 2010, **56**, 592
19 Yi TF, Xie Y and Zhu YR, *J Power Sources*, 2012, **211**, 59
20 Prabakar SJR, Han SC and Singh SP, *J Power Sources*, 2012, **209**, 57
21 Arrebola J, Caballero A and Hernán L, *J Power Sources*, 2010, **195**, 4278
22 Liu J and Manthiram A, *Chem Mater*, 2009, **21**, 1695
23 Wu HM, Belharouak I and Abouimrane A, *J Power Sources*, 2010, **195**, 2909
24 Lee Y, Mun J and Kim D-W, *Electrochim Acta*, 2014, **115**, 326
25 Fan Y, Wang J and Tang Z, *Electrochim Acta*, 2007, **52**, 3870
26 Li X, Guo W and Liu Y, *Electrochem Acta*, 2014, **116**, 278
27 Lin Y, Yang Y and Yu R, *J Power Sources*, 2014, **259**, 188
28 Kang HB, Myung ST and Amine K, *J Power Sources*, 2010, **195**, 2023
29 Liu D, Bai Y and Zhao S, *J Power Sources*, 2012, **219**, 333
30 Amatucci G, Blyr A and Sigala C, *Solid State Ionics*, 1997, **104**, 13
31 Eddrief M, Dzwonkowski P and Julien C, *Solid State Ionics*, 1991, **45**, 77
32 Soppe W, Aldenkamp F and Den Hartog H, *J Non-Cryst Solids*, 1987, **91**, 351

33 Ying J, Wan C and Jiang C, *J Power Sources*, 2001, **102**, 162
34 Dou J, Kang X and Wumaier T, *J Solid State Electrochem*, 2012, **16**, 1481
35 Şahan H, Göktepe H and Patat Ş, *Solid State Ionics*, 2008, **178**, 1837
36 Chan H-W, Duh J-G and Sheen S-R, *Surf Coat Technol*, 2004, **188-189**, 116
37 Chan HW, Duh JG and Sheen SR, *Electrochim Acta*, 2006, **51**, 3645
38 Jin Y C, Lin C Y and Duh J G, Electrochim Acta, 2012, **69**, 45
39 Wang L, Li H, Huang X, et al, Solid State Ionics, 2011, **193**, 32
40 Zhong Q, Bonakdarpour A, Zhang M, et al, J Electrochem Soc, 1997, **144**, 205
41 Liu GQ, Wen L and Wang X, *J Alloys Compd*, 2011, **509**, 9377
42 Xu GL, Xu YF and Fang JC, *ACS Appl Mater Interfaces*, 2013, **5**, 6316
43 Fu F, Xu G-L and Wang Q, *J Mater Chem A*, 2013, **1**, 3860
44 Yang M, Du C and Tang Z, *Ionics*, 2014, **20**, 1039
45 Xie J, Zhao X and Cao G, *J Power Sources*, 2005, **140**, 350